Ceramics International 45 (2019) 8017–8022

Contents lists available at ScienceDirect

Ceramics International

journal homepage: www.elsevier.com/locate/ceramint

Short communication

Enhancement of photocatalytic hydrogen production of $BiFeO_3$ by Gd^{3+} doping

Yuxuan Yang[a], Le Kang[b,*], Hui Li[a]

[a] College of Materials and Mineral Resources, Xi'an University of Architecture and Technology, Xi'an 710055,China
[b] College of Materials Science and Engineering, Xi'an University of Science and Technology, Xi'an 710055, China

ARTICLE INFO

Keywords:
$BiFeO_3$:Gd^{3+}
Photocatalytic activity
Magnetic properties

ABSTRACT

In order to investigate the influence of Gd^{3+} doping on the photocatalytic activity of $BiFeO_3$, $BiFeO_3$ and $BiFeO_3$:Gd^{3+} photocatalysts were fabricated by the sol-gel process. The phase, photocatalytic hydrogen production, microstructure, optical and photoelectrochemical properties of the fabricated photocatalysts were investigated. $BiFeO_3$:Gd^{3+} photocatalyst has a larger ability for the hydrogen production in photocatalysis process than that of $BiFeO_3$. The reason of the higher photocatalytic activity of $BiFeO_3$:Gd^{3+} photocatalyst was revealed by the measurements of UV–Vis diffuse reflectance spectra, photocurrent curves and electrochemical impedance spectra. Moreover, the magnetic properties of $BiFeO_3$ and $BiFeO_3$:Gd^{3+} photocatalysts were also investigated to show the easy separation. These results in current work indicate that $BiFeO_3$:Gd^{3+} is an excellent photocatalyst and has potential applications in photocatalytic hydrogen production.

1. Introduction

In recent years, sustainable energy is paid more and more attention due to its characteristics of economy, environmental friendliness and social benefits [1,2]. As one of sustainable energies, hydrogen (H_2) can approach challenges of greenhouse effect and environmental sustainability. And the photocatalytic production of H_2 and O_2 by water splitting using photocatalysts receives an impressive amount of attention because of its great economic and environmental interest [3]. In the process of photocatalytic H_2 production, electron-hole ($e^- - h^+$) pairs are generated when photons with energy higher than or equal to the band gap energy (E_g) hit the photocatalyst. The produced electrical charges are used to dissociate water. The process of photocatalytic water splitting contains photo reduction and photo oxidation reactions, which can be written as:

$$\text{Photo reduction:} 2H_2O + 2e^- \xrightarrow{h\nu} H_2 + 2OH^- \quad (1)$$

$$\text{Photo oxidation:} 2H_2O \xrightarrow{h\nu} O_2 + 4H^+ + 4e^- \quad (2)$$

Generally, the photocatalytic activity of a photocatalyst is determined by its light absorption, generation of $e^- - h^+$ pairs, recombination and separation of $e^- - h^+$ pairs, migration of $e^- - h^+$ pairs, charge carrier trapping and transfer of $e^- - h^+$ pairs to water [4].

It has been almost 50 years since Fujishima and Honda reported the water spilling to H_2 and O_2 using the TiO_2 photocatalyst [5,6]. Except for TiO_2, various types of photocatalysts were reported in these years, such as titanate [7,8], AM_2O_4 (A = Cu and Zn, M = Al, Cr, Mn, Fe and Co) [9,10], tantalite (niobate) [11,12], sulphide [13,14], ferrite [15,16] and some oxide semiconductor [17–22]. $BiFeO_3$ is a perovskite-type multiferroic compound, which shows potential applications in spintronics devices due to its high ferroelectric and magnetic phase transitions, as well as large remanent polarization at room temperature [23–25]. Moreover, it shows excellently photovoltaic effect and photocatalytic activity because that it can absorb a wide range of sunlight corresponding to its small E_g [26–28]. For the applications in the photocatalyst field, one of advantages of $BiFeO_3$ is its excellently magnetic property. It is known that the separation of photocatalysts is essential after the photocatalytic process. Generally, coagulation, flocculation and sedimentation are widely used in the separation process although they are complex and expensive [29,30]. But the separation process will be easy if the photocatalyst has the magnetism. It means that the photocatalyst can be separated easily by applying an exterior magnetic field.

There are some reports for $BiFeO_3$ in photocatalytic degradation of organic pollutants in water [27,28,31–37]. Chen's work shows that the hydrothermally-synthesized $BiFeO_3$ nanocrystals have excellently photocatalytic activity for methyl orange degradation under visible light irradiation and the surface oxygen vacancies enhance the

* Corresponding author.
E-mail address: jmhehou@sina.com (L. Kang).

https://doi.org/10.1016/j.ceramint.2018.12.150
Received 15 November 2018; Received in revised form 16 December 2018; Accepted 20 December 2018
Available online 21 December 2018
0272-8842/ © 2018 Elsevier Ltd and Techna Group S.r.l. All rights reserved.

photocatalytic activity effectively [37]. Other reports indicate that the photocatalytic activity of $BiFeO_3$ can be enhanced by doping ions, such as Sm and Mn [34,35], La and Se [36], and Gd [31–33]. However, little or no report keeps a watchful eye on the influence of ion doping on photocatalytic hydrogen production of $BiFeO_3$. In this work, we report the sol-gel synthesis and the photocatalytic hydrogen production of $BiFeO_3$ and $BiFeO_3$:Gd^{3+}. The results show that the photocatalytic hydrogen production can be increased by Gd^{3+} doping.

2. Materials and method

$BiFeO_3$ and $BiFeO_3$:Gd^{3+} were synthesized by a sol-gel method. The Gd^{3+} doping concentration is 5%mol. In the synthesis, $Bi(NO_3)_3{\cdot}5H_2O$ (99.0%), $Fe(NO_3)_3{\cdot}9H_2O$ (99.99%) and $Gd(NO_3)_3{\cdot}6H_2O$ (99.99%) were used as starting materials. Deionized water was used as the solvent. Citric acid and ethylene glycol were used as additives. In a typical synthesis of $BiFeO_3$:Gd^{3+}, 40 mL of ethylene glycol was mixed with 80 mL of deionized water under vigorous stirring for 20 min. Then, 2 g of Citric acid was added into the mixed solution under vigorous stirring for 20 min. Subsequently, 7.5 mmol of $Bi(NO_3)_3{\cdot}5H_2O$, 8 mmol of $Fe(NO_3)_3{\cdot}9H_2O$ and 0.5 mmol of $Gd(NO_3)_3{\cdot}6H_2O$ were added into the above solution under vigorous stirring for 120 min. The obtained solution was continuously stirred for 100 min at 80 ºC to form the sol. Finally, the formed sol was transferred into a culture dish and dried at 100 ºC till the gel was obtained and the obtained gel was calcined at 550 ºC for 120 min. The synthesis process of $BiFeO_3$ was similar with that of $BiFeO_3$:Gd^{3+}.

The phase was confirmed by a Rigaku D/max2550VB X-ray powder diffractometer at a voltage of 40 Kv and a current of 30 mA with Cu Kα radiation (λ = 1.54056 Å). The data were recorded in a 2θ angle of 20–70 º with a scan speed of 10 º/min. The microstructure was performed on a JSM-6700F scanning electron microscopy (SEM). The synthesized samples were dispersed in ethanol using an ultrasonicator and dropped on a carbon grid. The UV–Vis diffuse reflectance spectra (DRS) were obtained by a UV-2600 spectrophotometer (Shimadzu) using an integrating-sphere accessory in the light wavelength range of 200–800 nm and $BaSO_4$ was used as a reflectance standard. The hysteresis loops were recorded by a Vibrating Sample Magnetometer (Lakeshore VSM 7410) in the external field from -9T to +9T.

The photoelectrochemical measurements were performed on an electrochemical workstation (CHI 760E Chenhua Instrument Company, Shanghai, China) containing a standard three-electrode system. In the system, the Pt wire and Ag/AgCl (saturated KCl) were used as the counter and reference electrodes, respectively. A 300 W Xe arc lamp (PLS-SXE300C, Beijing Perfect Light Co. Ltd., Beijing) served as the light source, and 0.5 M Na_2S aqueous solution was used as the electrolyte.

The abilities of photocatalytic hydrogen production for $BiFeO_3$ and $BiFeO_3$:Gd^{3+} were evaluated in a batch reactor. 0.1 g of photocatalyst was dispersed in 100 mL of solution with the H_2O/CH_3OH volume ratio of 9:1. Before the photocatalysis, the reaction system was evacuated firstly by a mechanical pump and filled subsequently with N_2 for the purpose of removing O_2. The process was repeated 2 times. Then, the mixture was irradiated by the simulated sunlight. The generated H_2 was collected by the water displacement technique and the amount was measured by an online gas chromatograph.

3. Results and discussion

The single phase of the synthesized $BiFeO_3$ and $BiFeO_3$:Gd^{3+} was confirmed by the XRD technique. Fig. 1 gives the XRD patterns of $BiFeO_3$, $BiFeO_3$:Gd^{3+} and the standard data of JCPDs card no. 86–1518. The diffractions fit well with the standard data of JCPDs card no. 86–1518, which suggests the successful synthesis of $BiFeO_3$ and $BiFeO_3$:Gd^{3+} with rhombohedral structure (space group *R3c*). Due to the same valence and similar radii of Bi^{3+} (1.170 Å, CN = 8) and Gd^{3+} (1.053 Å, CN = 8) [38], Gd^{3+} ions substitute Bi^{3+} sites in $BiFeO_3$:Gd^{3+}. This substitution also can be revealed by the shifts of diffraction peaks to the larger angles. The substitution of smaller Gd^{3+} to Bi^{3+} leads to the decrease of lattice distance and thus induces the decrease of unit cell, which results in the shift of diffraction peaks to larger angles [39,40]. No signals for Gd element are detected, indicating that Gd^{3+} has doped into $BiFeO_3$ host entirely and formed solid state solution.

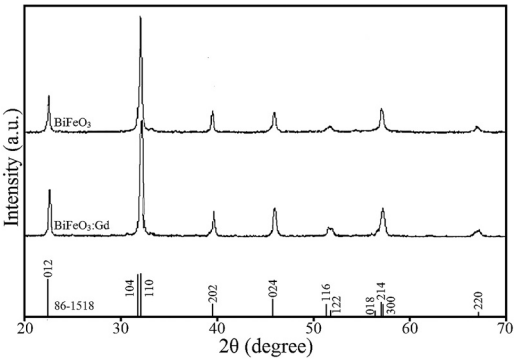

Fig. 1. XRD patterns of $BiFeO_3$ and $BiFeO_3$:Gd^{3+}, as well as the standard data of JCPDs no.86-1518.

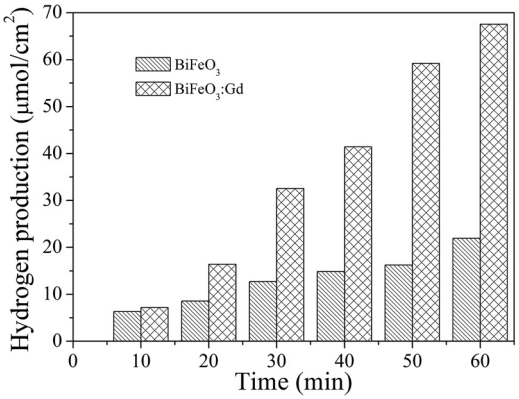

Fig. 2. Dependence of hydrogen production on irradiation time in the photocatalysis process with the presence of $BiFeO_3$ and $BiFeO_3$:Gd^{3+}.

Photocatalytic hydrogen production of the synthesized $BiFeO_3$ and $BiFeO_3$:Gd^{3+} was evaluated under the simulated sunlight irradiation using methanol as the hole-scavenger. Fig. 2 gives the dependence of hydrogen production on irradiation time in the photocatalysis process with the presence of $BiFeO_3$ and $BiFeO_3$:Gd^{3+}. The rates of hydrogen production for $BiFeO_3$ and $BiFeO_3$:Gd^{3+} are about 21.9 and 67.6 $\mu mol{\cdot}cm^{-2}{\cdot}h^{-1}$, respectively. It can be seen that the rate of $BiFeO_3$:Gd^{3+} is more than three times of the $BiFeO_3$. The results demonstrate that $BiFeO_3$:Gd^{3+} has a larger photocatalytic activity than that of $BiFeO_3$. It is known that the ability of hydrogen production for a particulate photocatalyst depends on its crystallinity, microstructure, optical and electronic properties [41]. To find out the mechanism of the higher photocatalytic activity of $BiFeO_3$:Gd^{3+}, a series of physical and chemical properties of $BiFeO_3$ and $BiFeO_3$:Gd^{3+} were investigated and compared.

Fig. 3 shows the microstructural analysis of $BiFeO_3$ (Fig. 3A) and $BiFeO_3$:Gd^{3+} (Fig. 3B). The SEM images show that a large number of

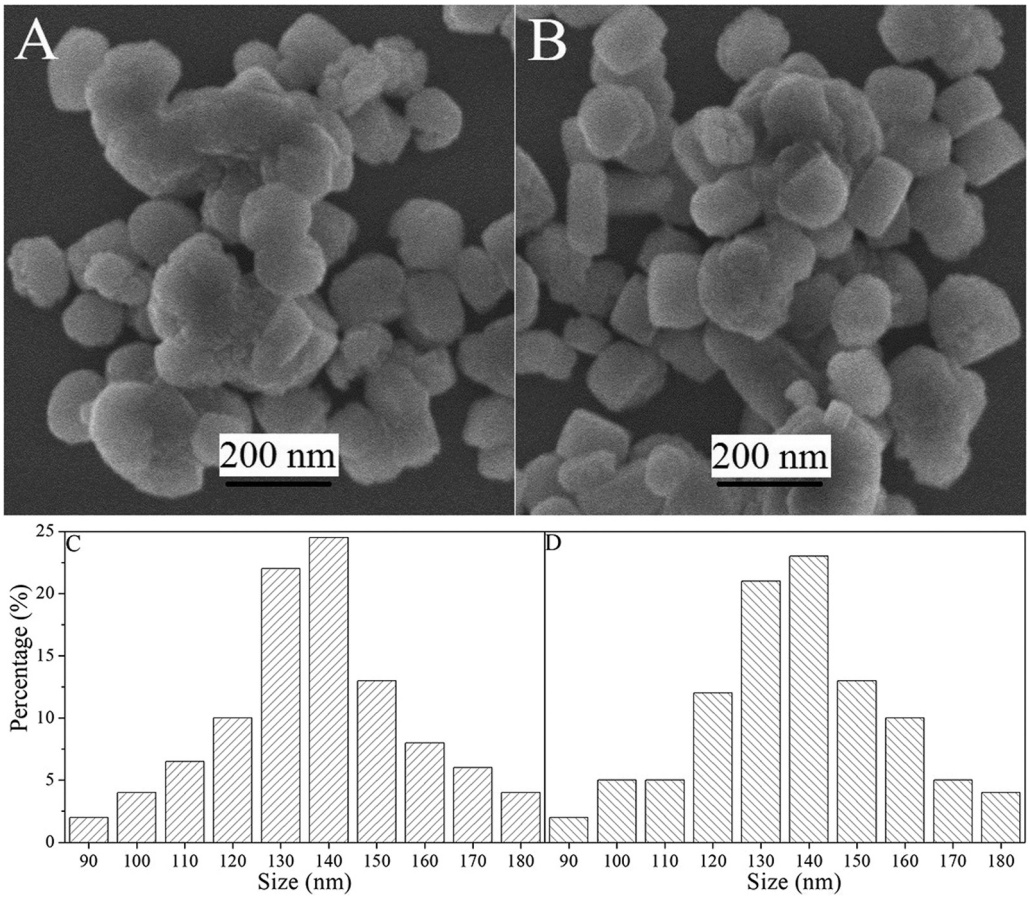

Fig. 3. SEM images and size distribution of $BiFeO_3$ (A and C) and $BiFeO_3$:Gd^{3+} (B and D).

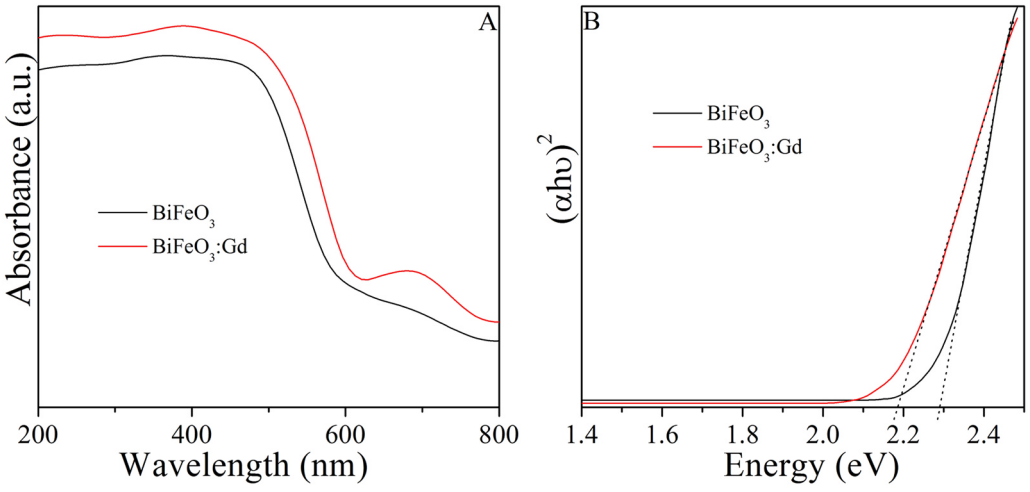

Fig. 4. UV–Vis DRS (A) and corresponding Tauc plots representing $(\alpha h\upsilon)^2$ vs E_g (B) of $BiFeO_3$ and $BiFeO_3$:Gd^{3+}.

irregular nanoparticles were produced by the sol-gel process. There are agglomerations between particles. But the agglomeration does not influence the band gap of samples [34]. In the sol-gel synthesis, the complexing ligands of precursor xerogel wrote over the produced nanocrystals and thus prevented the agglomeration. But the subsequent calcination induced the evaporation of citrate complexing agents. Thus, the nanocrystals agglomerated and grow to be larger due to their high surface energy. These led to the final microstructure of the synthesized photocatalysts. Fig. 3C and Fig. 3D provide the size distribution of $BiFeO_3$ and $BiFeO_3$:Gd^{3+}, respectively. The results indicate that the size

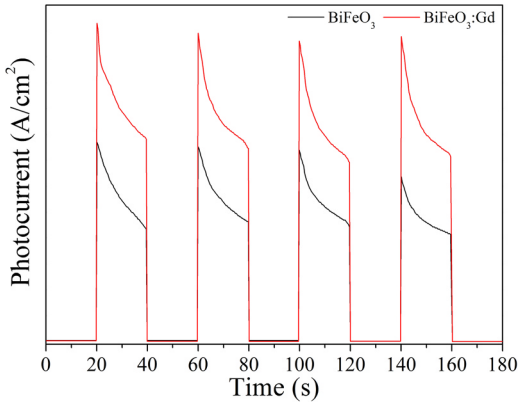

Fig. 5. Photocurrent curves of $BiFeO_3$ and $BiFeO_3$:Gd^{3+} in four on-off cycles under simulated sunlight irradiation.

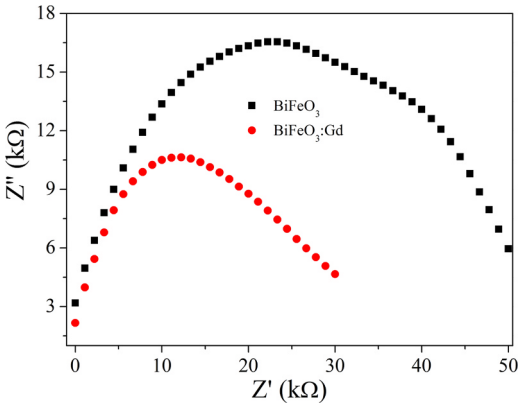

Fig. 6. EIS of $BiFeO_3$ and $BiFeO_3$:Gd^{3+}.

distribution is similar. The XRD an SEM results suggest the morphology, particle size and distribution of $BiFeO_3$ and $BiFeO_3$:Gd^{3+} are similar. Therefore, the effects of crystallinity and microstructure on photocatalytic activities of $BiFeO_3$ and $BiFeO_3$:Gd^{3+} are same.

The optical properties of the synthesized $BiFeO_3$ and $BiFeO_3$:Gd^{3+} were investigated. Fig. 4A gives the UV–Vis DRS of $BiFeO_3$ and $BiFeO_3$:Gd^{3+} in the wavelength range of 200–800 nm. $BiFeO_3$ shows the strong absorption band in ultraviolet light region and the weak absorption band in visible light region. $BiFeO_3$:Gd^{3+} has the same absorption bands with $BiFeO_3$, but the absorption intensities are higher than those of $BiFeO_3$. The absorption band in ultraviolet light region corresponds to charge transfer from valence O2p states to the conduction-band Fe3d states [42]. The absorption band in visible light region is induced by the vacancies of oxygen [43]. And the obvious enhancement of absorption intensity in visible light region for $BiFeO_3$:Gd^{3+} is induced by the increased vacancies of oxygen [44]. The results show that $BiFeO_3$:Gd^{3+} has a larger absorption capability and a longer wavelength of absorption band edge than that of $BiFeO_3$. The band gap energy was calculated by the Kubelka-Munk formula of $(\alpha h\nu) = A(h\nu - E_g)^{\frac{n}{2}}$, where α is the absorption coefficient, $h\nu$ is the photon energy, n is a constant having the values of 2 and 4 for direct and indirect band gaps, and A is a constant [45]. The results are shown in Fig. 4B. The calculated E_g for $BiFeO_3$ and $BiFeO_3$:Gd^{3+} are 2.28 and 2.17 eV, respectively. The E_g of $BiFeO_3$ is the measure of energy gap

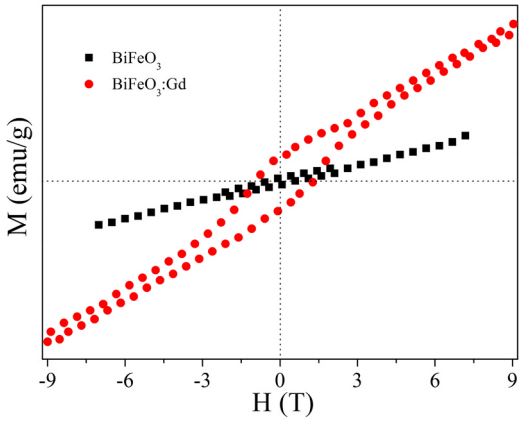

Fig. 7. Magnetization-magnetic field curves of $BiFeO_3$ and $BiFeO_3$:Gd^{3+}.

between the top of the O (2p)-Fe (3d) mixed valence-band and bottom of the Fe 3d conduction band [46]. Umebayashi et al. have found that the 3d metal doping leads to the generation of the occupied level in the valence band or the band gap because of the t_{2g} state of the doped ions [47,48]. The doped Gd^{3+} in $BiFeO_3$ induces the formation of impurity levels in the forbidden band, which leads to the shifts in the donor level above the original valence band or an acceptor level under the original conduction band [49]. These result in the decrease of E_g for $BiFeO_3$:Gd^{3+}. Moreover, the increased vacancies of oxygen in $BiFeO_3$:Gd^{3+} also result in the decrease of E_g [50].

For a photocatalyst, the effective generation, separation and recombination of $e^- - h^+$ pairs have obvious influence on photocatalytic activity. The generation, separation and recombination of $e^- - h^+$ pairs can be demonstrated by the photocurrent. Fig. 5 gives the photocurrent curves of $BiFeO_3$ and $BiFeO_3$:Gd^{3+} in four on-off cycles under simulated sunlight irradiation. The $BiFeO_3$:Gd^{3+} shows higher photocurrent intensity than that of $BiFeO_3$, which suggests the higher efficient generation and separation of $e^- - h^+$ pairs and the longer lifetime of charger carriers for $BiFeO_3$:Gd^{3+}. The charge separation of $e^- - h^+$ pairs on the interface of the photocatalyst also can be revealed by the electrochemical impedance spectra (EIS). And the reaction rate on the surface of the photocatalyst can be revealed by the radius of the EIS. The radius of EIS is smaller, the separation of $e^- - h^+$ pairs and the charger transfer across the electrode/electrolyte interface are more efficient [51]. Fig. 6 shows the EIS of $BiFeO_3$ and $BiFeO_3$:Gd^{3+} measured in the triode-electrode configuration with a sinusoidal alternating-current perturbation of 10 mV. The radius of the semicircle in the plot of $BiFeO_3$:Gd^{3+} is smaller, suggesting that Gd^{3+} doping benefits the separation of $e^- - h^+$ pairs and promotes the charger transfer across the electrode/electrolyte interface. The optical and photoelectrochemical properties demonstrate that the higher photocatalytic activity of $BiFeO_3$:Gd^{3+} in photocatalytic hydrogen production results from the efficient generation, separation and migration of $e^- - h^+$ pairs.

To investigate the magnetic properties of $BiFeO_3$ and $BiFeO_3$:Gd^{3+}, the magnetization-magnetic field (M-H) curves were measured at room temperature. The results are shown in Fig. 7. It can be seen that $BiFeO_3$ has a nearly linear magnetic field dependence on the magnetization but $BiFeO_3$:Gd^{3+} shows a hysteresis loop, which means a higher magnetic property of $BiFeO_3$:Gd^{3+}. And this suggests that $BiFeO_3$:Gd^{3+} can be separated easily after the photocatalysis process in the solution. The magnetic separation of $BiFeO_3$:Gd^{3+} was tested by placing a magnet beside the glass beaker. The samples were collected by the magnet in

30 s, suggesting that an easy and efficient way for the separation of $BiFeO_3$:Gd^{3+} in solution. The higher magnetic property of $BiFeO_3$:Gd^{3+} than that of $BiFeO_3$ can be attributed the following reasons [30]. Firstly, the substitution of smaller Gd^{3+} to Bi^{3+} results in the larger lattice distortion, which leads to the suppression of the spiral spin modulation. Secondly, the Gd^{3+}-Fe^{3+} couples in $BiFeO_3$:Gd^{3+} also induce the enhancement of magnetic property.

4. Conclusion

We fabricated $BiFeO_3$ and $BiFeO_3$:Gd^{3+} photocatalysts successfully through a sol-gel phase. The $BiFeO_3$:Gd^{3+} shows higher photocatalytic activity in hydrogen production than that of $BiFeO_3$. By the measurements of the phase, microstructure, optical and photoelectrochemical properties, we conclude that the higher photocatalytic activity of $BiFeO_3$:Gd^{3+} comes from the more efficient generation, separation and migration of $e^- - h^+$ pairs. By Gd^{3+} doping, the E_g becomes to be smaller; the absorption ability of sunlight becomes to be stronger; the separation and migration of $e^- - h^+$ pairs become to be more efficient. As a result, the photocatalytic activity is enhanced highly. The higher magnetic property of $BiFeO_3$:Gd^{3+} suggests that the collection in the solution is easier. The physical and chemical properties demonstrate that $BiFeO_3$:Gd^{3+} has potential application in photocatalytic hydrogen production.

References

[1] C. Acar, I. Dincer, G.F. Naterer, Review of photocatalytic water-splitting methods for sustainable hydrogen production, Int. J. Energy Res. 40 (2016) 1449–1473.
[2] H. Fu, Z. Li, Z. Liu, Z. Wang, Research on big data digging of hot topics about recycled water use on micro-blog based on particle swarm optimization, Sustainability 10 (2018) 2488.
[3] A.A. Ismail, D.W. Bahneman, Photochemical splitting of water for hydrogen production by photocatalysis: a review, Sol. Energy Mater. Sol. Cells 128 (2014) 85–101.
[4] H. Tong, S. Ouyang, Y. Bi, N. Umezawa, M. Oshikiri, J. Ye, Nano-photocatalytic materials: possibilities and challenges, Adv. Mater. 24 (2012) 229–251.
[5] A. Fujishima, K. Honda, Electrochemical photolysis of water at a semiconductor electrode, Nature 238 (1972) 37.
[6] A. Fujishima, K. Honda, Electrochemical evidence for the mechanism of the primary stage of photosynthesis, Bull. Chem. Soc. Jpn. 44 (1971) 1148–1150.
[7] F.T. Wagner, G.A. Somorjai, Photocatalytic hydrogen production from water on Pt-free $SrTiO_3$ in alkali hydroxide solutions, Nature 285 (1980) 559–560.
[8] D.W. Hwang, H.G. Kim, J.S. Lee, J. Kim, W. Li, S.K. Oh, Photocatalytic hydrogen production from water over M-doped $La_2Ti_2O_7$ (M = Cr, Fe) under visible light irradiation ($\lambda > 420$ nm), J. Phys. Chem. B 109 (2005) 2093–2102.
[9] S. Saadi, A. Bouguelia, M. Trari, Photoassisted hydrogen evolution over spinel CuM_2O_4 (M = Al, Cr, Mn, Fe and Co), Renew. Energy 31 (2006) 2245–2256.
[10] Y. Bessekhouad, M. Trari, Photocatalytic hydrogen production from suspension of spinel powders AMn_2O_4 (A= Cu and Zn), Int. J. Hydrog. Energy 27 (2002) 357–362.
[11] H. Kato, S. Kudo, Photocatalytic water splitting into H_2 and O_2 over various tantalate photocatalysts, Catal. Today 78 (2003) 561–569.
[12] S.M. Ji, P.H. Borse, H.G. Kim, D.W. Hwang, J.S. Jang, S.W. Bae, J.S. Lee, Photocatalytic hydrogen production from water–methanol mixtures using N-doped $Sr_2Nb_2O_7$ under visible light irradiation: effects of catalyst structure, Phys. Chem. Chem. Phys. 7 (2005) 1315–1321.
[13] Q. Li, H. Meng, J. Yu, W. Xiao, Y. Zheng, J. Wang, Enhanced photocatalytic hydrogen-production performance of graphene–$Zn_xCd_{1-x}S$ composites by using an organic S source, Chem. Eur. J. 20 (2014) 1176–1185.
[14] Y. Hou, Y. Zhu, Y. Xu, X. Wang, Photocatalytic hydrogen production over carbon nitride loaded with WS_2 as cocatalyst under visible light, Appl. Catal. B: Environ. 156–157 (2014) 122–127.
[15] S. Acharya, S. Mansingh, K.M. Parida, The enhanced photocatalytic activity of g-C_3N_4-$LaFeO_3$ for the water reduction reaction through a mediator free Z-scheme mechanism, Inorg. Chem. Front. 4 (2017) 1022–1032.
[16] A.K. Vishwakarma, P. Tripathi, A. Srivastava, A.S.K. Sinha, O.N. Srivastava, Band gap engineering of Gd and Co doped $BiFeO_3$ and their application in hydrogen production through photoelectrochemical route, Int. J. Hydrog. Energy 42 (2017) 22677–22686.
[17] M. Hara, T. Kondo, M. Komoda, S. Ikeda, J.N. Kondo, K. Domen, M. Hara, K. Shinohara, A. Tanaka, Cu_2O as a photocatalyst for overall water splitting under visible light irradiation, Chem. Commun. 0 (1998) 357–358.
[18] L. Liao, Q. Zhang, Z. Su, Z. Zhao, Y. Wang, Y. Li, X. Lu, D. Wei, G. Feng, Q. Yu, X. Cai, J. Zhao, Z. Ren, H. Fang, F. Robles-Hernandez, S. Baldelli, J. Bao, Efficient solar water-splitting using a nanocrystalline CoO photocatalyst, Nat. Nanotechnol. 9 (2014) 69–73.
[19] C.-C. Hu, H. Teng, Structural features of p-type semiconducting NiO as a co-catalyst for photocatalytic water splitting, J. Catal. 272 (2010) 1–8.
[20] X. Wang, Q. Xu, M. Li, S. Shen, X. Wang, Y. Wang, Z. Feng, J. Shi, H. Han, C. Li, Photocatalytic overall water splitting promoted by an α–β phase junction on Ga_2O_3, Angew. Chem. Int. Ed. 124 (2012) 13266–13269.
[21] Z.G. Zou, H. Arakawa, Direct water splitting into H_2 and O_2 under visible light irradiation with a new series of mixed oxide semiconductor photocatalysts, J. Photochem. Photobiol. A 158 (2003) 145–162.
[22] Z.G. Zou, J.H. Ye, K. Sayama, H. Arakawa, Direct splitting of water under visible light irradiation with an oxide semiconductor photocatalyst, Nature 414 (2001) 625–627.
[23] S. Pattanayak, B.N. Parida, P.R. Das, R.N.P. Choudhary, Impedance spectroscopy of Gd-doped $BiFeO_3$ multiferroics, Appl. Phys. A 112 (2013) 387–395.
[24] P. Suresh, P.D. Badu, S. Sinath, Role of (La,Gd) co-doping on the enhanced dielectric and magnetic properties of $BiFeO_3$ ceramics, Ceram. Int. 42 (2016) 4176–4184.
[25] M. Hasan, M.A. Basith, M.A. Zubair, Md Sarowar Hossain, R. Mahbub, M.A. Hakim, Md Fakhrul Islam, Saturation magnetization and band gap tuning in $BiFeO_3$ nanoparticles via co-substitution of Gd and Mn, J. Alloy. Compd. 687 (2016) 701–706.
[26] S.Y. Yang, L.W. Martin, S.J. Byrnes, T.E. Conry, S.R. Basu, D. Paran, L. Reichertz, J. Ihlefeld, C. Adamo, A. Melville, Y.-H. Chu, C.-H. Yang, J.L. Musfeldt, D.G. Schlom, J.W. Ager, R. Ramesh, Photovoltaic effects in $BiFeO_3$, Appl. Phys. Lett. 95 (2009) 062909.
[27] F. Gao, X.Y. Chen, K.B. Yin, S. Dong, Z.F. Ren, F. Yuan, T. Yu, Z.G. Zou, J.M. Liu, Visible-light photocatalytic properties of weak magnetic $BiFeO_3$ nanoparticles, Adv. Mater. 19 (2007) 2889–2892.
[28] X. Bai, J. Wei, B. Tian, Y. Liu, T. Reiss, N. Guiblin, P. Gemeiner, B. Dkhil, I.C. Infante, Size effect on optical and photocatalytic properties in $BiFeO_3$ Nanoparticles, J. Phys. Chem. C 120 (2016) 3595–3601.
[29] X. Cao, Y. Chen, S. Jiao, Z. Fang, M. Xu, X. Liu, L. Li, G. Pang, S. Feng, Magnetic photocatalysts with a p–n junction: Fe_3O_4 nanoparticle and $FeWO_4$ nanowire heterostructures, Nanoscale 6 (2014) 12366–12370.
[30] L. Kang, H.L. Du, H. Zhang, W.L. Ma, Systematic research on the application of steel slag resources under the background of big data, Complexity 2018 (2018) 6703908.
[31] R. Guo, L. Fang, W. Dong, F. Zheng, M. Shen, Enhanced photocatalytic activity and ferromagnetism in Gd doped $BiFeO_3$ nanoparticles, J. Phys. Chem. C 114 (2010) 21390–21396.
[32] S. Mohan, B. Subramanian, I. Bhaumik, P.K. Guota, S.N. Jaisankar, Nanostructured $Bi_{(1-x)}Gd_{(x)}FeO_3$ – A multiferroic photocatalyst on its sunlight driven photocatalytic activity, RSC Adv. 4 (2014) 16871–16878.
[33] N. Zhang, D. Chen, F. Niu, S. Wang, L. Qin, Y. Huang, Enhanced visible light photocatalytic activity of Gd doped $BiFeO_3$ nanoparticles and mechanism insight, Sci. Rep. 6 (2016) 26467.
[34] S. Irfan, Y. Shen, S. Rizwan, H.-C. Wang, S.B. Khan, C.-W. Nan, Band-gap engineering and enhanced photocatalytic activity of Sm and Mn doped $BiFeO_3$ nanoparticles, J. Am. Ceram. Soc. 100 (2017) 31–40.
[35] Z. Hu, D. Chen, S. Wang, N. Zhang, L. Qin, Y. Huang, Facile synthesis of Sm-doped $BiFeO_3$ nanoparticles for enhanced visible light photocatalytic performance, Mater. Sci. Eng. B 220 (2017) 1–12.
[36] S. Irfan, L. Li, A.S. Saleemi, C.-W. Nan, Enhanced photocatalytic activity of La^{3+} and Se^{4+} co-doped bismuth ferrite nanostructures, J. Mater. Chem. A 5 (2017) 11143–11151.
[37] D. Chen, F. Niu, L. Qin, S. Wang, N. Zhang, Y. Huang, Defective $BiFeO_3$ with surface oxygen vacancies: facile synthesis and mechanism insight into photocatalytic performance, Sol. Energy Mater. Sol. Cells 171 (2017) 24–32.
[38] R.D. Shannon, Revised effective ionic radii and systematic studies of interatomic distances in halides and chalcogenides, Acta Cryst. A32 (1976) 751–767.
[39] Y. Yang, B. Liu, Y. Zhang, X. Lv, L. Wei, J. Xu, H. Zhang, X. Wang, C. Zhang, J. Li, Influence of Mg^{2+}/Ga^{3+} doping on luminescence of $Y_3Al_5O_{12}$:Ce^{3+} phosphors, J. Mater. Sci.: Mater. Electron. 29 (2018) 17154–17159.
[40] Y. Yang, X. Lv, L. Wei, J. Xu, H. Yu, Y. Hu, H. Zhang, B. Liu, X. Wang, Q. Li, Energy transfer from Ce^{3+} to Eu^{3+} through Tb^{3+} chain in YPO_4:Ce^{3+}/Tb^{3+}/ Eu^{3+} phosphors, Solid State Commun. 269 (2018) 35–38.
[41] K. Maeda, Photocatalytic water splitting using semiconductor particles: history and recent developments, J. Photochem. Phottobiol. C 12 (2011) 237–268.
[42] S. Jiang, M. Lian, C. Lu, Q. Gu, S. Ruan, X. Xie, Ensemble prediction algorithm of anomaly monitoring based on big data analysis platform of open-pit mine slope, Complexity 2018 (2018) 1048756.
[43] A.M. Yang, X.L. Yang, J.C. Chang, B. Bai, F.B. Kong, Q.B. Ran, Research on a fusion scheme of cellular network and wireless sensor networks for cyber physical social systems, IEEE Access 6 (2018) 18786–18794.
[44] X. Chen, H. Zhang, T. Wang, F. Wang, W. Shi, Optical and photoluminescence properties of $BiFeO_3$ thin films grown on ITO-coated glass substrates by chemical solution deposition, Phys. Status Solidi 209 (2012) 1456–1460.
[45] P. Kubelka, Ein Beitrag Zur Optik der Farbanstriche (Contribution to the optic of paint), Z. fur Tech. Phys. 12 (1931) 593–601.

[46] R.N. Lakshmana, S. Emin, M. Valant, M.V. Shankar, Nanostructured Bi_2O_3@TiO_2 photocatalyst for enhanced hydrogen production, Int. J. Hydrog. Energy 42 (2017) 6627–6636.
[47] T. Umebayashi, T. Yamaki, H. Itoh, K. Asai, Analysis of electronic structure of 3d transition metal-doped TiO_2 based on band calculation, J. Phys. Chem. Solids 63 (2002) 1909–1920.
[48] A.M. Yang, S.S. Li, H.L. Lin, D.H. Jin, Edge extraction of mineralogical phase based on fractal theory, Chaos Soliton Fract. 117 (2018) 215–221.
[49] X. Chen, S. Shen, L. Guo, S.S. Mao, Semiconductor-based photocatalytic hydrogen generation, Chem. Rev. 110 (2010) 6503–6570.
[50] P.S. Basavarajappa, B.N.H. Seethya, NagarajuGanganagappa, K.B. Eshwaraswamy, R.R. Kakarla, Enhanced photocatalytic activity and biosensing of gadolinium substituted $BiFeO_3$ nanoparticles, ChemistrySelect 3 (2018) 9025–9033.
[51] S.J. Hong, S. Lee, J.S. Jang, J.S. Lee, Heterojunction $BiVO_4$/WO_3 electrodes for enhanced photoactivity of water oxidation, Energy Environ. Sci. 4 (2011) 1781–1787.